Journal of Materials Chemistry C

PAPER

View Article Online
View Journal | View Issue

Plasmonic optical sensors printed from Ag–PVA nanoinks†

Cite this: J. Mater. Chem. C, 2014, 2, 908

Rafael Abargues,*[a] Pedro J. Rodriguez-Canto,[b] Sandra Albert,[a] Isaac Suarez[b] and Juan P. Martínez-Pastor*[b]

In this paper we report on the use of a nanocomposite based on silver nanoparticles embedded in PVA as a plasmonic optical sensor to detect and quantify trace amounts of amines in gas and water, respectively. The transduction mechanism of the sensor is based on the changes of the LSPR band of Ag NPs when analyte molecules are chemisorbed on their surface. The Ag–PVA sensors are fabricated by means of a high-precision microplotter, a direct-write technology developed for printing materials from solution. The nanoink is formulated with a metal precursor ($AgNO_3$) and a polymer (PVA) using an adequate mixture of solvents to meet the rheological requirements for the fluid dispensing process. The LSPR intensity is the most sensitive magnitude to follow the interaction between Ag NPs embedded in PVA and amines. Ag–PVA patterns are tested as a plasmonic optical sensor for the detection of ethylenediamine in solution showing a limit of detection as low as 0.1 nM. Moreover Ag nanocomposite patterns are also used for sensing vapours of several biogenic (cadaverine and putrescine) and synthetic (ethylenediamine and methylenediamine) amines, where shorter amines exhibit the largest sensor response. This plasmonic optical sensor is also tested in real-time monitoring of chicken meat spoilage at room temperature. We believe that the Ag–PVA nanocomposite can be the basis for the development of sensor spots, bar-codes and other labels for smart packaging technology, among other sensing applications.

Received 13th August 2013
Accepted 13th November 2013

DOI: 10.1039/c3tc31596g

www.rsc.org/MaterialsC

Introduction

Molecular sensing and detection based on surface plasmons have attracted intense interest for detection of biomolecules with high sensitivity and low cost. This implies unique properties in terms of subwavelength light confinement, strong near electromagnetic field enhancement or high sensitivity to the local environment with potential applications not only in sensing, but also in photovoltaics and other disciplines.[1–5]

Ag and Au metal nanoparticles (NPs) exhibit the localized surface plasmon (LSPR) band at visible wavelengths. This is of great importance since plasmon excitation can be accessible by standard optical sources and methods. The size, shape and assembly of noble metal NPs mainly rule their optical properties.[6–8] Moreover, LSPR strongly depends on the refractive index of the surrounding environment (substrates, solvents and adsorbates) of NPs.[2–4,7,9] Based on this, Ag and Au NPs are gaining more and more attention as LSPR-based optical sensors. Adsorption of molecules on the metal surface can lead to measurable spectral changes in both the wavelength and intensity of the LSPR.[4,10–13] This high sensitivity allows LSPR sensors to become a powerful analytical platform. The most popular plasmonic sensor is based on the SPR occurring at the surface of gold thin films that have been chemically functionalized (*e.g.* Biacore sensors).[9,14–16] However, these systems have size restrictions, because it is difficult to fabricate a large-scale array format including the microfluidics and the optics associated with light excitation–detection. In this context, Van Duyne and co-workers achieved significant advances by means of the fabrication of solid-state LSPR-based biosensors based on 2D arrays of triangular silver/gold nanostructures obtained by means of polystyrene nanosphere lithography, being the closest approach to SPR devices at the nanoscale.[4,17] Other authors used more conventional lithographic techniques followed by metal evaporation for the fabrication of metallic nanostructures for chemical LSPR sensing[18] and selective deposition of metal nanoparticles from colloidal solution on functionalized substrates.[19] Matsui *et al.*[20] reported the use of molecularly imprinted polymers with embedded Au NPs as sensors. This nanocomposite sensing mechanism is based on the variable proximity of the Au NPs (particle–particle plasmon coupling) immobilized in the imprinted polymer, which exhibits selective binding of a given analyte accompanied by swelling that causes a LSPR blue-shift. Nevertheless, all these sensors based on either metal nanostructures or NPs still need multi-step and complex processes for their fabrication that would increase the final cost of both the sensor transducer and reading instrument.

[a]Intenanomat S.L., C/Catedrático José Beltrán 2, 46980 Paterna, Spain. E-mail: Rafael.Abargues@uv.es

[b]Instituto de Ciencia de los Materiales, Universidad de Valencia, P.O. Box 22085, 46071 Valencia, Spain

† Electronic supplementary information (ESI) available. See DOI: 10.1039/c3tc31596g

Recently, we proposed a novel LSPR sensing platform based on a nanocomposite thin film of Ag nanoparticles embedded in a polymer matrix such as polyvinyl alcohol (PVA)[21] and novolak.[22] Ag NPs are *in situ* synthesized inside the host polymers by a one-step procedure yielding high performance nanocomposites due to good dispersion of the NPs into the polymer matrix.[23,24] As a result, the LSPR of Ag NPs can be combined with the extraordinary range of properties of polymeric materials (*i.e.* transparency, processability, low-cost and lithographic capabilities).[25–27] We demonstrated chemosensing capabilities of the Ag–PVA nanocomposite to 2-mercaptoethanol with a limit of detection (LOD) below 20 nM. Other authors have also proposed the use of Ag–PVA films to sense Hg metal ions[28] and hydrogen peroxide.[29]

One of the major trends in the area of sensors is directed towards their miniaturization, because this is effective to obtain higher sensitivity, lower LOD and faster binding rate[30] and forms the basis for the fabrication of lab-on-a-chip systems. Actually, we have already demonstrated chemosensing capabilities of Ag–novolak micropatterns fabricated by photolithography which were also demonstrated in a previous study,[22] which forms the basis for the microfabrication of bio and chemo-chip sensors. However, miniaturization of sensors carried out by conventional lithographic techniques is often seen as time-consuming and very expensive processes that utilize very expensive and sophisticated clean room facilities with complicated technological procedures. Direct printing of functional materials from solution is an efficient alternative to conventional lithographic plus deposition techniques for producing photonic, electronic and optoelectronic devices.[31] Inkjet printing has emerged as an attractive patterning technique of novel functional materials such as metal nanoparticles, quantum dots, graphene, carbon nanotubes and conducting polymers,[32–36] because it exhibits significant advantages, such as low cost, high-speed patterning and applicability to various substrates.

In the present paper, we report on the fabrication of Ag–PVA sensors by means of a high-precision microplotter, as a direct-write technology developed for printing materials from solution. The core of the microplotter is a dispenser that uses controlled ultrasonics to deposit very small amounts of fluid on multitude of substrates in a non-contact manner. Microplotter systems are significantly different from the existing inkjet technology and offer some advantages in comparison with inkjet printing like better pattern resolution (5 μm instead of 20–50 μm) and easier ink formulation.[37,38] For the microplotter printing of the LSPR sensor, we have properly formulated the nanocomposite precursor solution by varying the amounts of both PVA and $AgNO_3$ and choosing an adequate solvent mixture of ethanol and water. After the printing procedure, the patterns are baked and the NPs are *in situ* synthesized inside the polymer. In this paper we extend the sensing capabilities of printed Ag–PVA micropatterns to the detection of amine-based analytes both in solution and in vapor. Sensing of amine species is of special importance for the freshness control of food and beverage products,[39–41] but also for environmental and industrial monitoring applications. The present study is directed to the detection of different synthetic (methylenediamine (MDA) and ethylenediamine (EDA)) and biogenic (putrescine (PUT) and cadaverine (CAD)) diamines both in solution and in the vapour phase. We demonstrate chemosensing capabilities of this nanocomposite against EDA in solution with a LOD $\approx$ 0.1 nM using the intensity decay of the LSPR band as a sensing parameter. Moreover, the response of Ag–PVA nanocomposite patterns was also tested against the exposure to the vapours of MDA, EDA, PUT and CAD. The largest response was obtained for shorter diamines. Finally, we tested the Ag–PVA sensor as a plasmonic optical nose for real-time monitoring of food freshness. Because the ultimate goal of sensors is to work under real-world conditions, we exposed the Ag–PVA sensor to vapours released by the spoilage of 50 g chicken breast stored at room temperature, as a proof of concept. We observed that after 48 hours, the Ag–PVA sensors experienced a noticeable colour change from yellow to nearly colourless. This work confirms that a fully disposable sensing platform technology can be developed using solution-processed metal–polymer nanomaterials, which may also form the basis for the development of smart packaging solutions.

Experimental

Materials and apparatus

Polyvinyl alcohol (average molecular weight: 130 000, 85% hydrolysed), methylenediamine, ethylenediamine, putrescine, cadaverine and $AgNO_3$ were purchased from Aldrich and used without further purification.

Ag–PVA nanocomposite preparation and device fabrication

We have properly formulated the nanocomposite precursor solution by varying the amounts of both PVA and $AgNO_3$ and choosing an adequate solvent mixture to meet the rheological requirements. The composition of the nanoink consists of a solution of 0.03 M $AgNO_3$ and 1 wt% of PVA in ethanol–water (1 : 3). Fig. 1a illustrates all the steps involved in the generation of Ag–PVA structures The nanoink solution is loaded into the dispenser and deposited onto a glass substrate by means of a SonoPlot® GIX Microplotter II based on an ultrasonic fluid dispensing head to generate the nanocomposite patterning. Afterwards, the sample is baked at 160 °C for 10 min to synthesize *in situ* the Ag NPs inside the PVA.[21,22,25] The film thickness of the resulting samples was measured to be around 160 nm by using a mechanical profilometer (Veeco Dektack 150).

Characterization techniques

Generation of Ag NPs inside PVA was confirmed by UV-vis spectroscopy with a commercially available reflectometer (Nanocalc 2000 from Ocean Optics Inc.) to correlate their optical properties with the size and shape of nanoparticles and their particle dispersion in the polymer matrix. Transmission electron microscopy (TEM) studies of the particles were also carried out at an accelerating voltage of 100 kV using a JEOL 1010 microscope. TEM samples were prepared by ultrasonicating very small pieces of BK7 in acetone with the corresponding nanocomposite thin film spin coated on it. With this procedure we obtained micrometre-sized pieces of the

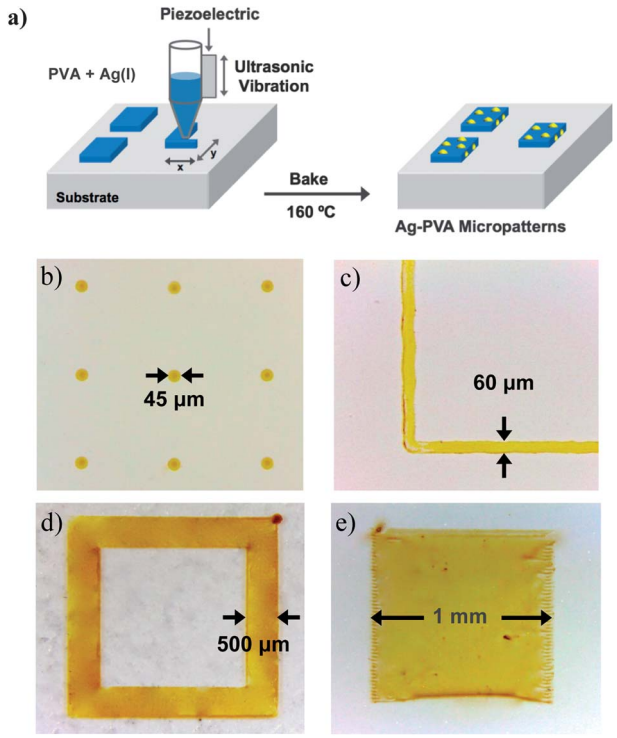

Fig. 1 (a) Scheme of the fabrication of the Ag–PVA nanocomposite sensor by microplotter printing. (b–e) Different patterns of Ag–PVA fabricated by microplotter printing.

corresponding nanocomposites in suspension in acetone. This suspension was dropped on a carbon-coated Cu grid. The viscosity and surface tension of the nanoink were measured at 25 °C using a rotational viscosimeter (Brookfield DV-I) and a du Nouy ring tensiometer (Kruss, Type K6) respectively.

Analyte detection protocol

Ag–PVA 1 mm^2 patterns were immersed in 40 mL of the EDA solution for different times. The calibration curve of EDA solution was determined using a different Ag–PVA sensor for every concentration. To limit the experimental error of using a different sensor and estimate the LOD more accurately we always chose an area wherein the LSPR intensity was approximately the same value. The exposure of the LSPR sensor to amines can also be performed by exposing the nanocomposite to the vapours of a 40 mL 0.1 M aqueous solution of amine (methylenediamine, ethylenediamine, cadaverine and putrescine) in a closed vessel of 100 mL in a thermostatic bath at 40 °C. Each spectrum was registered for different times once the liquid–vapour equilibrium is restored after closing the vessel. All UV-vis spectra were carefully obtained using a positioning system to measure in the same position of the sensor and achieve accurate and representative values of LSPR intensity.

Results and discussion

Ag–PVA sensor microfabrication

Printable nanocomposites have potential applications at all levels in optoelectronics and integrated photonics/plasmonics. Fig. 1a illustrates all the steps involved in the generation of Ag–PVA structures.

Once the nanocomposite precursor fluid is deposited to form a given pattern, the resulting patterns are baked on a hotplate for several minutes and Ag nanoparticles are *in situ* synthesized inside PVA. The formation of NPs consists of the chemical reduction of Ag(I) to Ag(0) by means of the oxidation of PVA.[42]

The microplotter printing performance is mainly determined by an adequate nanoink formulation. Functional inks must accomplish some physicochemical requirements such as viscosity and surface tension, which are the most important parameters.[43,44] For example, viscosity plays a key role in the resolution of lines[45] whereas the wetting properties of the ink on the substrate surface and solvent evaporation are also important to improve homogeneity of the printed structure and avoid the "coffee ring effect".[46] We formulated the nanocomposite precursor solution by varying the amounts of both PVA and $AgNO_3$ and choosing an adequate solvent mixture. Moreover, we took into account that for sensing purposes a narrow LSPR bandwidth is needed to achieve a precise quantification of the LSPR spectrum variations in response to the analyte binding to the Ag NPs. As previously reported,[21] optical properties of Ag–PVA nanocomposites depend on both the concentration of PVA and $AgNO_3$. Based on this criterion, we found that the optimal composition of the nanocomposite precursor solution contains 1 wt% PVA and 0.03 M $AgNO_3$ in EtOH–H_2O 1 : 3, whereas the ideal bake conditions were found to be 160 °C for 600 s. The viscosity and surface tension of the nanoink were measured to be 9.0 mPa s and 40.1 mN m^{-1} at 25 °C, respectively. Once the film is deposited and baked, the final composition is 75 wt% PVA and 25 wt% Ag.

Fig. 1b–e show white light optical microscope images of different Ag–PVA patterns printed on glass substrates from the optimized ink formulation. We printed four types of microstructures with different feature sizes from 45 µm to 1 mm, as examples of this printing technique for the present chemosensor applications. After the bake step at 160 °C all the patterns exhibit a vivid yellow colour due to the LSPR related absorption, which is characteristic of the formation of Ag NPs inside the polymer. The synthesis of Ag NPs within the PVA matrix can be followed by UV-vis spectroscopy (see ESI†). Once the reaction is finished after baking at 160 °C for 10 min, the resulting Ag–PVA nanocomposite structures showed a symmetric and narrow plasmonic absorption band centred at 420 nm. We observe by TEM images that Ag NPs are spherical and uniformly distributed within the polymer matrix and have a mean diameter of 10.8 ± 2.9 nm (see ESI†).

LSPR sensing of amines in solution

Ag–PVA patterns fabricated by microplotter printing were tested as optical sensors sensitive to local changes in the environment of Ag NPs when the analyte molecules are chemisorbed on their surface. The sensor consists of a 1 mm^2 square pattern (Fig. 1e), because this size allowed the use of a conventional optical setup to measure the LSPR absorption of such a Ag–PVA pattern. Furthermore, we extend here the sensing capabilities of Ag–PVA

nanocomposites (previously reported for 2-mercaptoethanol[21]) to the detection of amine analytes, such as methylenediamine (MDA), ethylenediamine (EDA), putrescine (PUT) and cadaverine (CAD) (see ESI†). Diamines are well-known chelating ligands for coordination to metals through N atoms *via* their lone pairs of electrons that interact with Ag NPs.[47]

Initially, we carried out the sensing studies of the amine-based analyte in aqueous solution. The protocol followed for the analyte binding consists of the immersion of the Ag–PVA nanocomposite patterns into a solution of the analyte molecules to be detected. Fig. 2a shows the evolution of the absorption spectrum of an Ag–PVA pattern for different immersing times into a 10^{-4} M EDA aqueous solution. As can be observed, the LSPR band is very sensitive to the adsorption of amines on Ag NPs. The LSPR of the Ag–PVA pattern significantly changes in intensity and slightly in wavelength and linewidth when exposed to the analyte for a given time.

We observe an induction period around 1.5 min before the LSPR intensity starts to decay. As PVA swelling is a relatively slow process compared to analyte diffusion, we expect this initial delay for the sensor response. After 65 min the LSPR band is 10% of the initial intensity and shows a wavelength red-shift of 10.7 nm and an increase in the linewidth of 171 nm. From a nanoscopic point of view, after sensing we did not observed a significant change on the Ag NPs size (see ESI†). In order to obtain more precise values of the LSPR peak intensity, curves were fitted by Lorentzian functions. The gradual intensity reduction of the LSPR is explained by the increase of attached EDA molecules on the surface of Ag NPs embedded in the PVA matrix. In comparison, the immersion of the Ag–PVA pattern into water for 250 min (inset of Fig. 2a) only produced a negligible change in the LSPR band.

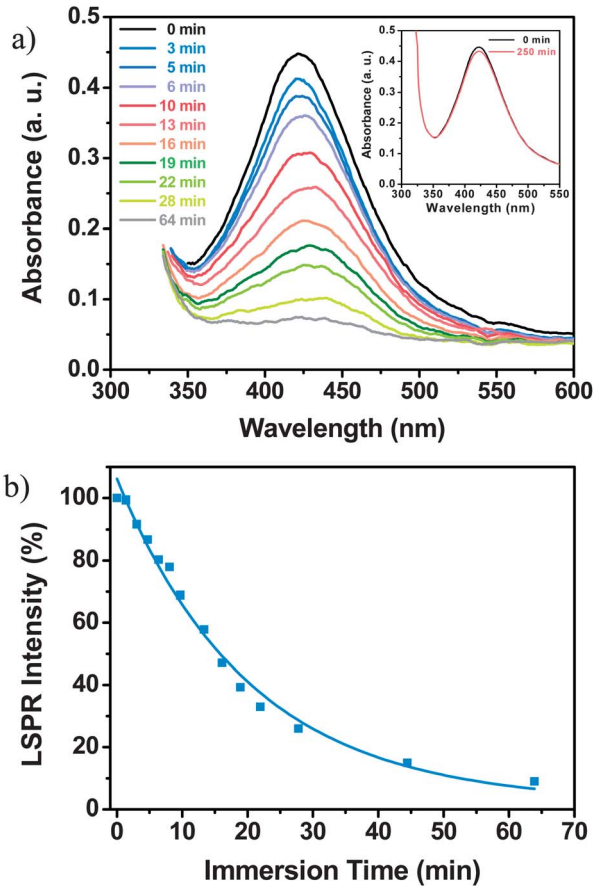

Fig. 2 Real time response of the sensor to 10^{-4} M ethylenediamine aqueous solution. (a) LSPR curves for different immersing times of the nanocomposite. Inset: sensor response to water and (b) decrease in LSPR peak intensity as a function of the immersing time and a fitting exponential curve accounting for the analyte diffusion.

It is worth mentioning that the binding of EDA molecules on Ag NPs is irreversible: the analyte cannot be desorbed to return the nanosensor to its initial state. This is not, however, a limitation because the present Ag–PVA nanosensors (even if fabricated as microarrays) are easy-to-prepare, easy-to-use and inexpensive, which are the basis of a fully disposable sensing platform technology, in contrast to other commonly used SPR sensing platforms.[48] As reported by Hu *et al.*, ethylenediamine shows affinity for Ag NPs *via* its two N atoms.[47] There are two proposed mechanisms to explain the decrease in the LSPR intensity. The first one is the decrease in the electron density in the valence band of Ag NPs. This has been better studied for the case of thiols, where the 4d electrons of the silver atoms are transferred to the sulphur atom of the thiol, leaving a lower concentration of free electrons in the Ag NP for the plasmon resonance.[49] The second mechanism consists of the increase of the plasmon resonance damping constant due to charge localization at the surface of the Ag NP, namely chemical-interface damping.[50,51] Both mechanisms are present in the EDA–nanoparticle interaction given that the LSPR linewidth increases monotonically, but at slower rate (a factor two, from 0.75 to 1.5 eV) than the increase of the peak intensity (a factor six, from 1 to 0.17 in normalized units). In fact, the integrated intensity (proportional to the product of the peak intensity and linewidth) is approximately constant during the first 30 min, which would indicated that the damping mechanism dominates in this time interval, whereas the charge transfer mechanism does at longer times.

The real-time kinetic response of Ag–PVA to an EDA concentration solution of 10^{-4} M as a function of immersion time is represented using the LSPR intensity (Fig. 2b) as a response variable. Experimental data can be fitted by the following saturating function:

$$A_t = A_\infty + B\mathrm{e}^{-kt} \quad (1)$$

where A_t is the absorption intensity at a given time, A_∞ is the saturation LSPR intensity and k is the binding rate constant. From the fit of the LSPR intensity *vs.* time (Fig. 2b) to eqn (1) we found $k = 0.82 \pm 0.11$ ms^{-1} and $A_\infty = 2.1 \pm 1.0\%$. As can be seen in Fig. 2b, we observed that the LSPR peak intensity evolves as a function of the immersing time. Analyte binding to Ag NPs is a strongly time-dependent phenomenon, which is determined by the analyte mass transport and the subsequent chemical interaction rate.[52] Initially, the analyte molecules must be transported from the bulk solution to the Ag NP surface. It is well-known that PVA is a hydrogel that gradually swells in the aqueous medium

and can retain a certain amount of water without dissolving. Therefore, water and analyte diffusion inside the Ag–PVA nanocomposite is allowed.[53] As PVA swelling is a relatively slow process compared to analyte diffusion, we observe an induction time of 1.5 min before the LSPR intensity starts to decay. In our previous work,[21] we showed that after water swelling of PVA, analyte diffusion is large enough to allow a nearly constant analyte concentration in the nanocomposite structure and the analyte binding takes place at the surface of all metal NPs. On the other hand, the net binding reaction rate (slope of the curve at any point) will mainly depend on the amount of available NPs (binding sites) into the PVA matrix and the size and concentration of the analyte. The Ag–PVA sensor presents a cumulative response to an analyte over time until all binding sites are occupied. The highest binding rate is achieved at the beginning of the reaction. As a result, the relative importance of mass transport and chemical interaction can change during the course of detection: mass transport processes can be limiting at the beginning of the sensing test while interaction limits the observed binding rate at later stages.

Fig. 3 presents the sensor response to different analyte concentrations for a constant immersion time of 250 min for the whole tested range of the EDA concentration in order to ensure that analyte binding is complete. Calibration curves for analyte binding assays are generally characterized by a sigmoidal relationship between the sensor response and the analyte concentration. The four-parameter logistic (4PL) function was used for fitting the concentration–response, because it is recognized as the reference standard for immunoassays such as ELISAs or dose–response curves.[54] The equation describing the 4PL function is:[55]

$$A = A_\infty + \frac{(A_0 - A_\infty)}{1 + (C/C_{1/2})^s} \quad (2)$$

in which A is the LSPR intensity response, A_∞ is the response at infinite analyte concentration, A_0 is the response at zero analyte concentration, C is the analyte concentration, $C_{1/2}$ is the concentration of analyte necessary to produce a response of 50%, and s is the slope at $C_{1/2}$ of the calibration curve.

As can be observed in Fig. 3, Ag–PVA structures exhibit a limit of detection (LOD) to EDA around 0.1 nM, which is equivalent to 0.2 ng or 6 ppt. We estimate that the number of Ag NPs in a 1 mm^2 sensor pattern with a thickness of 160 nm to be around 10^{11} NPs, assuming a complete reduction of Ag(I) to Ag(0), a NP size of 10.8 nm and a PVA density of 1.3 g cm^{-3}. From the LOD found for EDA, we estimate that the minimum sensor response is achieved for a ratio of analyte to Ag NP around 20. This ratio would be easily reduced by just reducing the film thickness of the sensor. The maximum sensor response, that is, the saturating value of the sensor, is achieved for analyte concentrations around 10^{-3} M and an estimated NP : analyte ratio around 10^6. The linear detection range for EDA was determined to be over an analyte concentration of six orders of magnitude, from 10^{-10} to 10^{-4} M (inset of Fig. 3). The sensitivity was determined to be 14.6 ± 1.0% from the slope of the linear regression of the calibration curve shown in the inset of Fig. 3. Here the sensitivity is defined as the sensor response per logarithmic unit of analyte concentration. From the calibration curve, we can also determine the binding affinity (K_A), which is the equilibrium binding constant and measures the propensity of the analyte to bind reversibly to the sensor. Under the assumption of a linear relationship between sensor occupancy and response, the binding affinity is equal to the inverse of $C_{1/2}$.[56,57] Thus, we found that $C_{1/2} = 250 \pm 70$ nM and $K_A = (4.1 \pm 1.2)10^6$ M^{-1}. The higher the value of K_A, the higher affinity between sensor and analyte and the less analyte is required to achieve 50% occupancy of the sensor's binding sites.

Based on these results, our system is expected to be effective for quantitative sensing of EDA molecules within a very broad range. Further improvement of the LOD can be achieved by the sensor miniaturization, because the ratio of analyte molecules to Ag NPs is therefore increased and a higher sensor response is reached. Because the binding rate decreases significantly for low analyte concentrations, a modification of the sensing protocol would be necessary to achieve faster binding rates by, for example, carrying out the binding reaction at higher temperatures.

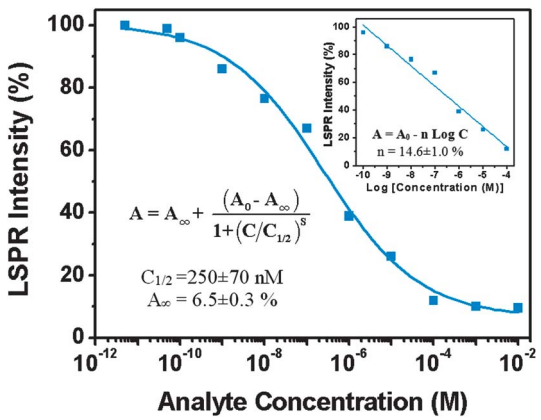

Fig. 3 Absorption decay response of the Ag–PVA sensor as a function of the EDA concentration for an immersion time of 250 min. Inset: linear dependence and the corresponding regression line of the sensor response.

LSPR sensing of amines in vapour phase

The response of the Ag–PVA was also performed by exposing the nanocomposite patterns to the vapours of different diamines (Fig. 4). The sensing protocol consisted of the exposure of Ag–PVA to the resulting amine vapour from 40 mL of a saturated amine aqueous solution (0.1 M) in a closed vessel of 100 mL in a thermostatic bath at 40 °C. A given concentration of analyte will be in the vapour phase depending on the vapour pressure of the corresponding amine once the liquid–vapour equilibrium is reached. This concentration can be estimated by Raoult's law ($p_a = p_a^* x_a$, where p_a is the partial pressure of the analyte in the solution), p_a^* is the vapour pressure of the pure analyte and x_i is the mole fraction of the analyte in the mixture) assuming that analyte–H_2O behaves as an ideal solution (Table 1). Given that the tested amines have different vapour pressures, molecular length and affinities for metal surfaces we expect different sensor responses.

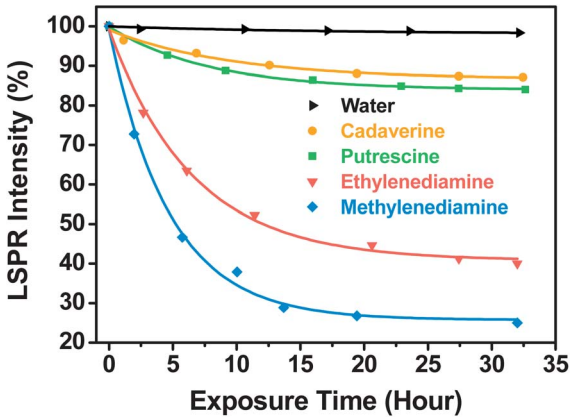

Fig. 4 Variation of the LSPR peak intensity exposed to the vapours of a 0.1 M aqueous solution of methylenediamine, ethylenediamine, putrescine and cadaverine.

Fig. 4 shows the real-time sensor response to vapours of different diamines and water. Every time that a measurement is carried out, the liquid–vapour equilibrium is broken. Therefore, for the next measurement it is necessary to wait until the equilibrium is restored and this indeed takes several hours. Because the analyte solution is saturated, we can assume a constant concentration of the analyte in solution throughout the experiment. After exposure to analyte vapour, analyte molecules diffuse into the Ag–PVA nanocomposite. Experimental data were fitted to eqn (1) and the resulting fitting parameters (saturating LSPR intensity and kinetic binding constant) are listed in Table 1.

We notice that the response of Ag–PVA to water vapour was fully negligible, which indicates no interaction between H_2O and Ag NPs in PVA. On the other hand, we measure a different sensor response to the different amines tested. This can be explained in terms of the analyte relative pressure in the vapour phase, their molecular length and their affinity for Ag NPs.

Moreover, MDA shows the highest binding rate constant ($58.7 \pm 1.2\ \mu s^{-1}$) followed by EDA ($42.4 \pm 1.5\ \mu s^{-1}$), PUT ($35.6 \pm 1.0\ \mu s^{-1}$) and CAD ($28.7 \pm 0.8\ \mu s^{-1}$). The largest response is obtained for shorter diamines because these molecules are more volatile and therefore their concentration in the vapour phase is higher. Thus, we estimate that the maximum concentration of MDA and EDA in the gas phase was 7.6 and 1.2 μM, respectively, whereas those of larger molecules, PUT and CAD, were 0.25 and 0.09 μM. It must be pointed out that these concentrations were calculated from Raoult's law assuming that binary solution diamine–H_2O behaves as an ideal solution. In fact, the actual vapour pressure of diamines is indeed less than expected, because the system amine–water shows a negative deviation from Raoult's law due to the formation of strong intermolecular H-bonds.[58] As a result, the solute–solvent interactions are stronger than those in pure solute and pure solvent and the volatility of amines decreases. The concentration of EDA in the vapour phase can also be estimated experimentally from the calibration curve shown in Fig. 3, even though this curve was obtained from the analyte in solution. For a sensor response of 40.8% the detected EDA concentration would be 1.05 μM. In fact, this value can be more realistic than that calculated from Raoult's law (1.2 μM), according to the overestimation explained above.

LSPR sensing for real-time monitoring of food freshness

One of the most promising applications of gas sensors is in the food industry. Biogenic amines such as putrescine, cadaverine and other S-containing compounds have an important role as indicators of quality in some foods.[39–41] Given that the Ag–PVA nanocomposite is able to detect both amines and S-containing compounds, the Ag–PVA sensor may be used as a plasmonic optical nose for real-time monitoring of food freshness. The ultimate goal and challenge of sensors is to work under real-world conditions. As a proof of concept, we exposed the 25 mm^2 square Ag–PVA sensor to 50 g chicken breast stored in a Petri dish at room temperature.

Fig. 5 shows the Ag–PVA sensor response to chicken for three different exposure times. Chicken meat spoilage leads to the production of a wide variety of volatile compounds, including hydrogen sulphide, dimethyl disulphide, indole, ammonia, putrescine, cadaverine and other biogenic amines.[41] Upon exposure, we observed a gradual colour change of the sensor from yellow to nearly colourless within the first 24 hours, which can be followed by the naked eye.

UV-vis spectroscopy confirms a significant decrease in the LSPR band intensity after 24 hours (see ESI†) as previously demonstrated for pure amines. Moreover, a smaller Ag–PVA square pattern (0.25 mm^2 in area) exhibited a maximum response after 18 hours (see ESI†) because of the smaller surface sites for analyte binding and hence this sensor will exhibit higher sensitivity and lower LOD. This means that the sensor response to food spoilage can be easily tuned by means of the nanocomposite size and thickness depending on the detection level to be reached.

Table 1 Kinetic binding constants and maximum absorption decay for Ag–PVA sensors exposed to vapour of various diamines and water

Analyte	Vapour pressure[a] [mmHg]	$[Analyte]_{vap.}$[a] [μM]	k [μs^{-1}]	LSPR abs. [%]
Water	—	—	—	99.0 ± 0.2
Methylenediamine	78.1	7.62	58.7 ± 1.2	25.7 ± 1.4
Ethylenediamine	12.1	1.21	42.4 ± 1.5	40.8 ± 1.0
Putrescine	2.56	0.25	35.6 ± 1.0	83.9 ± 0.2
Cadaverine	0.96	0.09	28.7 ± 0.8	86.7 ± 0.8

[a] At 25 °C.

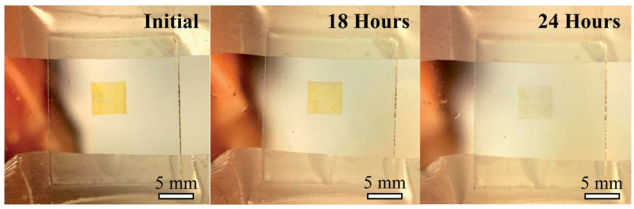

Fig. 5 Optical images before and after exposure to chicken meat for 18 and 24 hours.

Given that the Ag–PVA nanocomposite can be printed on different substrates, the Ag–PVA sensor can be easily incorporated into the food package. Therefore, a smart packaging technology may be developed on this material for the naked-eye colorimetric control of food and beverage freshness. The plasmonic optical nose shown here can be alternatively formulated on the basis of the synthesis of the Ag–Au alloyed nanoparticle to give more intense colours, for example. More quantitative measurements could be easily developed using a simple sensing device based on a commercially available and low-cost violet LED emitting at 405 nm and a filtered photodetector to measure with higher precision the colour intensity changes in real time.

Conclusions

In this paper we demonstrated the use of 1 mm^2 square patterns of the Ag–PVA nanocomposite fabricated by microplotter printing as a plasmonic sensor to detect and quantify trace amounts of amines in water and gas. We showed chemosensing capabilities of Ag–PVA patterns against EDA in solution and found a LOD of 0.1 nM, this is 0.3 ng or 6 ppt. We also observed a linear sensing behaviour within a concentration range between 10^{-10} and 10^{-4} M, which allows us to use Ag–PVA as a quantitative sensor for EDA. Secondly, we successfully tested the LSPR response of Ag–PVA patterns to the vapours of several amines in thermal equilibrium. The largest response was obtained for shorter diamines because these molecules are more volatile and therefore their concentration in the vapour phase is higher. Finally, the Ag–PVA plasmonic optical sensor was tested for real-time monitoring of chicken meat spoilage at room temperature. After 24 hours at room temperature we observed by the naked eye a noticeable colour change of the Ag–PVA label from yellow to colourless because of the increasing amount of volatile compounds released during the chicken spoilage.

This work confirms that a fully disposable sensing platform technology can be developed from solution-processed PVA containing metal nanoparticles and used as plasmonic optical sensors. Because Ag–PVA patterns can be easily fabricated with different shapes and dimensions on several substrates (glass, plastic, glossy paper, *etc.*), we believe that the metal NP–polymer nanocomposite can be the basis for the development of plasmonic tongue and nose, sensor spots, bar-codes and other labels for smart packaging technology, to perform chemosensing in several fields such as food industry, environmental monitoring (*i.e.* detection of volatile organic compounds (VOCs) and heavy metals in air, water and soil samples), health (*i.e.* detection of lung cancer with VOC markers in the breath) and security (*i.e.* detection of explosives and chemical weapons). Although the LSPR can be used as a qualitative colorimetric sensor, simple and cost-effective optical devices can be easily designed for quantitative and portable reading platforms.

Acknowledgements

This work was supported through the Generalitat Valenciana Grant PROMETEO/2009/074 and the Spanish MINECO project TEC2011-29120-C05-01. Intenanomat also thanks the FEDER Grant IMCBTA/2010/82 from IMPIVA.

Notes and references

1 S. A. Maier, M. L. Brongersma, P. G. Kik, S. Meltzer, A. A. G. Requicha and H. A. Atwater, *Adv. Mater.*, 2001, **13**, 1501.
2 H. Wang, Y. Wu, B. Lassiter, C. L. Nehl, J. H. Hafner, P. Nordlander and N. J. Halas, *Proc. Natl. Acad. Sci. U. S. A.*, 2006, **103**, 10856–10860.
3 S. Link and M. A. El-Sayed, *Annu. Rev. Phys. Chem.*, 2003, **54**, 331.
4 J. N. Anker, W. P. Hall, O. Lyandres, N. C. Shah, J. Zhao and R. P. Van Duyne, *Nat. Mater.*, 2008, **7**, 442.
5 E. Pedrueza, J. L. Valdés, V. Chirvony, R. Abargues, J. Hernández-Saz, M. Herrera, S. I. Molina and J. P. Martínez-Pastor, *Adv. Funct. Mater.*, 2011, **21**, 3502–3507.
6 K. S. Lee and M. A. El-Sayed, *J. Phys. Chem. B*, 2006, **110**, 19220.
7 K. L. Kelly, E. Coronado, L. L. Zhao and G. C. Schatz, *J. Phys. Chem. B*, 2003, **107**, 668.
8 R. Abargues, S. Albert, J. L. Valdés, K. Abderrafi and J. P. Martínez-Pastor, *J. Mater. Chem.*, 2012, **22**, 22204–22211.
9 M. E. Stewart, C. R. Anderton, L. B. Thompson, J. Maria, S. K. Gray, J. A. Rogers and R. G. Nuzzo, *Chem. Rev.*, 2008, **1080**, 494.
10 P. J. Rodríguez-Cantó, M. Martínez-Marco, F. J. Rodríguez-Fortuño, B. Tomás-Navarro, R. Ortuño, S. Peransí-Llopis and A. Martínez, *Opt. Express*, 2011, **19**, 7664–7672.
11 F. J. Rodríguez-Fortuño, M. Martínez-Marco, B. Tomás-Navarro, R. Ortuño, J. Martí, A. Martínez and P. J. Rodríguez-Cantó, *Appl. Phys. Lett.*, 2011, **98**, 133118.
12 R. W. Bogue, *Sens. Rev.*, 2004, **24**, 253.
13 K. A. Willets and R. P. Van Duyne, *Annu. Rev. Phys. Chem.*, 2007, **58**, 267.
14 J. Homola, *Chem. Rev.*, 2008, **108**, 462–493.
15 S. Scarano, M. Mascini and A. P. F. Turner, *Biosens. Bioelectron.*, 2010, **25**, 957–966.
16 J. M. Brockman, B. P. Nelson and R. M. Corn, *Annu. Rev. Phys. Chem.*, 2000, **51**, 41.
17 C. L. Haynes and R. P. Van Duyne, *J. Phys. Chem. B*, 2001, **105**, 5599.
18 M. P. Raphael, J. A. Christodoulides, S. P. Mulvaney, M. M. Miller, J. P. Long and J. M. Byers, *Anal. Chem.*, 2012, **84**, 1367–1373.

19 P. L. Truoang, B. W. Kim and S. J. Sim, *Lab Chip*, 2012, **12**, 1102.
20 J. Matsui, K. Akamatsu, S. Nishiguchi, D. Miyoshi, H. Nawafune, K. Tamaki and N. Sugimoto, *Anal. Chem.*, 2004, **76**, 1310.
21 R. Gradess, R. Abargues, A. Habbou, J. Canet-Ferrer, E. Pedrueza, A. Russell, J. L. Valdés and J. P. Martínez-Pastor, *J. Mater. Chem.*, 2009, **19**, 9233–9240.
22 J. Marqués-Hueso, R. Abargues, J. L. Valdés and J. P. Martínez-Pastor, *J. Mater. Chem.*, 2010, **20**, 7436–7443.
23 S. Porel, S. Singh, S. S. Harsha, D. N. Rao and T. P. Radhakrishnan, *Chem. Mater.*, 2005, **17**, 9.
24 G. V. Ramesh, S. Porel and T. P. Radhakrishnan, *Chem. Soc. Rev.*, 2009, **38**, 2646.
25 R. Abargues, K. Abderrafi, E. Pedrueza, R. Gradess, J. Marqués-Hueso, J. L. Valdés and J. P. Martínez-Pastor, *New J. Chem.*, 2009, **33**, 1720.
26 R. Abargues, J. Marqués-Hueso, J. Canet-Ferrer, E. Pedrueza, J. L. Valdés, E. Jiménez and J. P. Martínez-Pastor, *Nanotechnology*, 2008, **19**, 355308.
27 J. Marqués-Hueso, R. Abargues, J. Canet-Ferrer, S. Agouram, J. L. Valdés and J. P. Martínez-Pastor, *Langmuir*, 2010, **26**(4), 2825–2830.
28 G. V. Ramesh and T. P. Radhakrishnan, *ACS Appl. Mater. Interfaces*, 2011, **3**(4), 988–994.
29 E. Filippo, A. Serra and D. Manno, *Sens. Actuators, B*, 2009, **138**, 625–630.
30 A. B. Dahlin, *Sensors*, 2012, **12**, 3018–3036.
31 M. Singh, H. M. Haverinen, P. Dhagat and G. E. Jabbour, *Adv. Mater.*, 2010, **22**, 673–685.
32 J. Perelaer, A. W. M. De Laat, C. E. Hendriks and U. S. Schubert, *J. Mater. Chem.*, 2008, **18**, 3209.
33 V. Wood, M. J. Panzer, J. Chen, M. S. Bradley, J. E. Halpert, M. G. Bawendi and V. Bulović, *Adv. Mater.*, 2009, **21**, 2151–2155.
34 F. Torrisi, T. Hasan, W. Wu, Z. Sun, A. Lombardo, T. S. Kulmala, G. W. Hsieh, S. Jung, F. Bonaccorso, P. J. Paul, D. Chu and A. C. Ferrari, *ACS Nano*, 2012, **6**, 2992–3006.
35 H. Okimoto, T. Takenobu, K. Yanagi, Y. Miyata, H. Shimotani, H. Kataura and Y. Iwasa, *Adv. Mater.*, 2010, **22**, 3981–3986.
36 Y. Y. Noh, N. Zhao, M. Caironi and H. Sirringhaus, *Nat. Nanotechnol.*, 2007, **2**(12), 784–789.
37 B. J. Larson, S. D. Gillmor and M. G. Lagally, *Rev. Sci. Instrum.*, 2004, **75**, 832–836.
38 S. H. Ko, H. Pan, C. P. Grigoropoulos, C. K. Luscombe, J. M. J. Frechet and D. Poulikakos, *Appl. Phys. Lett.*, 2007, **90**, 141103.
39 G. Vinci and M. L. Antonelli, *Food Control*, 2002, **13**, 519–524.
40 C. Ruiz-Capillas and F. Jimenez-Colmenero, *Crit. Rev. Food Sci. Nutr.*, 2004, **44**, 489–499.
41 Y. Salinas, J. V. Ros-Lis, J. L. Vivancos, R. Martínez-Máñez, M. D. Marcos, S. Aucejo, N. Herranz and I. Lorente, *Analyst*, 2012, **137**, 3635–3643.
42 R. Abargues, R. Gradess, J. Canet-Ferrer, K. Abderrafi, J. L. Valdés and J. Martínez-Pastor, *New J. Chem.*, 2009, **33**, 913.
43 P. Calvert, *Chem. Mater.*, 2001, **13**, 3299–3305.
44 B. Derby, *Annu. Rev. Mater. Res.*, 2010, **40**, 395–414.
45 B. J. Larson, S. D. Gillmor and M. G. Lagally, *Rev. Sci. Instrum.*, 2004, **75**, 832–836.
46 C. Kim, M. Nogi, K. Suganuma and Y. Yamato, *ACS Appl. Mater. Interfaces*, 2012, **4**, 2168–2173.
47 G. Hu, Z. Feng, J. Li, G. Jia, D. Han, Z. Liu and C. Li, *J. Phys. Chem. C*, 2007, **111**, 11267–11274.
48 BIACORE is a trade mark. More information about these systems can be found in http://www.biacore.com.
49 G. C. Lica, B. S. Zelakiewicz, M. Constatinescu and Y. Y. Tong, *J. Phys. Chem. B*, 2004, **108**, 19896.
50 M. A. García, J. de la Venta, P. Crespo, J. Llopis, S. Penadés, A. Fernández and A. Hernando, *Phys. Rev. B: Condens. Matter Mater. Phys.*, 2005, **78**, 241403.
51 P. Crespo, R. Litrán, T. C. Rojas, M. Multigner, J. M. de la Fuente, J. C. Sánchez-López, M. A. García, A. Hernando, S. Penadés and A. Fernández, *Phys. Rev. Lett.*, 2004, **93**, 087204.
52 D. G. Myszka, *Curr. Opin. Biotechnol.*, 1997, **8**, 50–57.
53 A. Hasimi, A. Stavropoulou, K. G. Papadokostaki and M. Sanopoulou, *Eur. Polym. J.*, 2008, **44**, 4098.
54 J. W. A. Findlay, W. C. Smith, J. W. Lee, G. D. Nordblom, I. Das, B. S. DeSilva, M. N. Khan and R. R. Bowsher, *J. Pharm. Biomed. Anal.*, 2000, **21**, 1249–1273.
55 M. A. O'Connell, B. A. Belanger and P. D. Haaland, *Chemom. Intell. Lab. Syst.*, 1993, **20**, 97–114.
56 L. S. Jung, J. S. Shumaker-Parry, C. T. Campbell, S. S. Yee and M. H. Gelb, *J. Am. Chem. Soc.*, 2000, **122**, 4177–4184.
57 T. Kenakin, *Trends Pharmacol. Sci.*, 2004, **25**, 186–192.
58 N. G. McDuffie, *Langmuir*, 2001, **17**, 5711–5713.